THE JOURNAL OF PHYSICAL CHEMISTRY C
A JOURNAL OF THE AMERICAN CHEMICAL SOCIETY

pubs.acs.org/JPCC
Article

ReaxFF Parameter Set for Boron Clusters and Icosahedral Boron Crystals: Comparison with Density Functional Theory and Machine-Learning Potentials

Amin Ahmadisharaf,* Adri C. T. van Duin, Bin Liu, Dylan Evans, Sadra Sabouri, and Jeffrey Comer*

Cite This: J. Phys. Chem. C 2025, 129, 22319−22333
Read Online

ABSTRACT: Icosahedral boron materials, which include regular icosahedra of 12 boron atoms have gained increasing attention due to their potential applications as superhard materials, semiconductors, and energy storage media. However, the synthesis of high quality crystals of these materials has been a major barrier to the development of these applications. To enable computational prediction of synthesis conditions yielding high-quality icosahedral boron crystals, herein we tested and refined a set of ReaxFF parameters for the nucleation and growth of such crystals. We focused on matching the relative energies of small boron clusters obtained by density functional theory since such small clusters and similar motifs are likely present in crystal nuclei and at the interface of growing crystals. Using a training set of B_{80} clusters, including a low-energy core−shell structure containing a B_{12} icosahedron core and a high-energy single-shell structure produced in preliminary ReaxFF simulations, the ReaxFF parameter set was refined to better reproduce energies calculated by density functional theory (DFT). Among existing ReaxFF parameter sets and the machine-learning interatomic potentials MACE-MP-0, MACE-MP-0b3, MACE-MPA-0, PFP v7.0.0, and SevenNet-MF-ompa, only our new parameter set and PFP v7.0.0 correctly ranked these B_{80} clusters. This refinement led to improved agreement with DFT for a test set of 58 clusters consisting of 8−103 boron atoms. Furthermore, our refined parameter set yielded greater local icosahedral structure than the previously existing ReaxFF parameter set for larger scale simulations of crystallization from supercooled liquid boron. Additionally, simulations of solid boron in contact with molten nickel using our refined ReaxFF parameters yielded a boron solubility value that agrees moderately well with experimental expectations, while the previous boron parameters gave a value that was much too low.

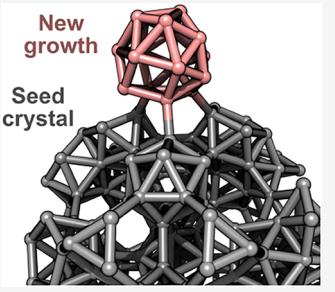

INTRODUCTION

Elemental boron and boron-rich compounds, such as boron carbide (B_4C), boron suboxide (B_6O), and boron subphosphide $B_{12}P_2$, have remarkably complex unit cells including multiple B_{12} icosahedra—that is, 12 boron atoms lying at the vertices of a regular icosahedron with B−B bond distances of about 1.75 Å. These B_{12} icosahedra are interconnected by interstitial boron atoms or heteroatoms, such as metals, oxygen, arsenic, phosphorus, or carbon, creating extended three-dimensional networks. The stability of the B_{12} icosahedra is made possible by three-center bonds having considerable electron density in the center of the triangles making up the icosahedra.[1] Icosahedral boron materials, including icosahedral boron arsenide ($B_{12}As_2$), are potential candidates for betavoltaics, which efficiently convert nuclear radiation directly to electrical power.[2] There are many applications for such betavoltaics, especially in space or deep-sea applications where accessing and replacing batteries can be very expensive. The long lifespan of nuclear batteries also makes them suitable for medical devices such as pacemakers.[3]

High-quality crystals, with low defect densities or controlled densities of specific defects, are needed for betavoltaics and electronics applications.[3,4] Growing such high quality crystals is challenging and current methods require high pressure, which increases the cost and limits the ability to scale up.[5] Metal flux methods have the potential to enable the synthesis process near atmospheric pressure with low densities of defects.[6] Exploring and optimizing these alternative synthesis techniques could pave the way for more cost-effective and scalable production of high-quality crystals.

Experimentally finding conditions that promote the growth of high-quality crystals is costly and time-consuming, and could be accelerated by guidance from computation. Modeling and simulation can provide this guidance, while also giving insight on atomic-scale mechanisms of growth. Nevertheless, boron is probably the most difficult of all pure elements to model, given the wide variety of bond geometries it can adopt. Boron is a unique element, as it is the only member of its group that is not a metal (the next congener being aluminum), likely due to the frustrated nature of covalent bonding in group 13. Group 14 elements up to and including tin in its gray allotrope tend toward 4-coordinate structures, which can be satisfied by tetrahedral

Received: July 11, 2025
Revised: October 16, 2025
Accepted: October 27, 2025
Published: November 4, 2025

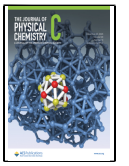

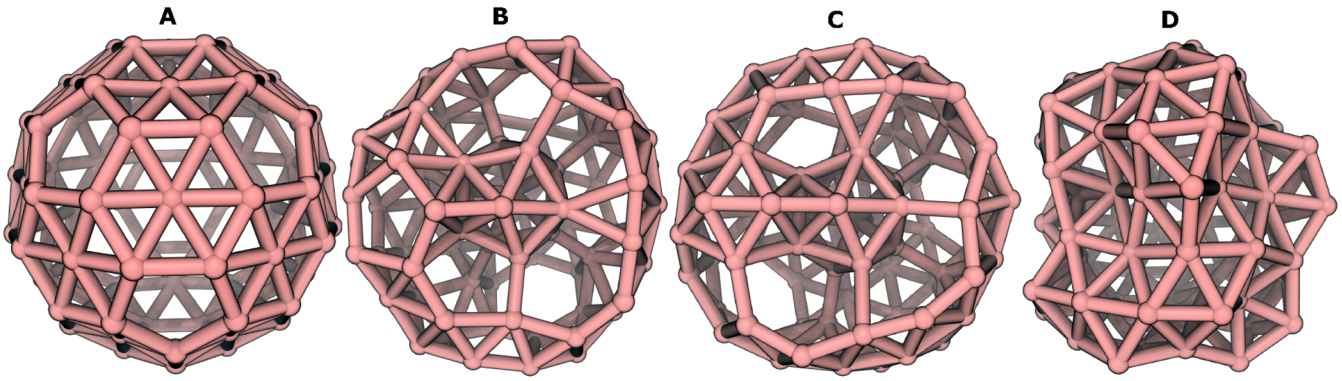

Figure 1. Four B_{80} structures considered for training and validation of the ReaxFF parameter set. (A) The B_{80} buckyball of Gonzalez Szwacki et al.,[36] having a structure similar to the C_{60} buckyball of carbon (truncated icosahedron), except with an additional boron atom inserted at the center of each of the hexagonal faces. (B) The Zhao et al.[40] core−shell structure includes a B_{12} icosahedron in the core, which is lower energy. (C) A similar core−shell structure, obtained by De et al.,[42] which is the lowest energy B_{80} cluster known. (D) A dubious B_{80} cluster that appeared in simulations with an early version (Version 1) of our ReaxFF parameter set, which we call the "Pouch".

centers in the diamond structure. Group 15 elements phosphorus, arsenic, and antimony form various 3-coordinate structures (molecular tetrahedra as in white phosphorus or pleated honeycomb sheets in black phosphorus and gray arsenic). On the other hand, the expected 5-coordination of boron does not correspond to any simple extended structure, and isolated B_{12} icosahedra are not stable. Hence, boron allotropes have uniquely large and complex unit cells. The unit cell of the lowest energy allotrope, β-rhombohedral boron, contains 315 atoms of 15 inequivalent types. Motifs in this structure include: interconnected B_{12} icosahedra with 6-coordinate atoms (5 bonds within the icosahedron and 1 exterior), 6-coordinate bipyramidal bridging atoms, and fused triple icosahedra (B_{28}), each with 8-coordinate atoms at shared edges and a central 9-coordinate atom.[7] α-rhombohedral boron, another common allotrope, consists purely of interconnected B_{12} icosahedra, with an alternating pattern of 6- and 7-coordinate atoms. While carbon and phosphorus also exhibit a variety of allotropes, their lowest-energy structures (graphite and black phosphorus) are relatively simple. Moreover, among binary compounds, boron-rich icosahedral boron compounds also have the most complex structures known: the yttrium boride YB_{66} has a lattice constant of 23.4 Å and includes $(B_{12})_{13}$ supericosahedra formed from icosahedral clustering of 12 simple B_{12} icosahedra around one central B_{12} icosahedron.[8] The wide variety of coordination geometries present in such boron crystals, 2D borophenes,[9−11] and small boron clusters,[12,13] are challenging to represent with empirical potentials.

Because the unit cells of icosahedral boron compounds are so intricate and contain many atoms, the time scales necessary for the growth of even a single unit cell can be relatively long, likely on time scales of many nanoseconds or microseconds. This extended time scale makes it infeasible to directly simulate crystal growth using quantum methods, such as density functional theory (DFT). Ab initio molecular dynamics simulations (AIMD) on the subnanosecond time scale by Jakse and Pasturel[14] showed that liquid and undercooled boron exhibit pronounced short-range order built from "inverted umbrella" pentagonal-pyramid units, similar to the coordination of boron in the B_{12} icosahedra. In their simulations, the fraction of atoms in inverted-umbrella motifs rises substantially as the system cooled from 2360 to 2000 K, but no complete B_{12} icosahedra nor repeating crystal units were observed in these subnanosecond simulations.

In contrast, the ReaxFF framework can efficiently describe chemical processes, including changes in the covalent bond network and crystal nucleation and growth.[15−17] Previous studies have included classical reactive simulations of boron and boron compounds using ReaxFF[18,19] or Tersoff[20] potentials. Existing ReaxFF parameter sets were parametrized to reproduce DFT energies for continuous solid boron phases such as β-rhombohedral (β-B), as well as small boranes;[21] however, simulating crystal growth from a boron melt or boron in liquid metal solvents requires the representation of interfaces between liquid phases and solid boron, as well as small nuclei and clusters. Therefore, we sought to determine if existing ReaxFF parameters could provide a reliable representation of boron clusters and growing interfaces of icosahedral boron crystals.

Machine-learning interatomic potentials (MLIPs), typically trained from DFT data, have recently emerged as an alternative means to simulate chemical systems with performance many orders of magnitude faster than *ab initio* methods.[22−24] These potentials leverage advanced regression techniques to accurately interpolate energy landscapes and atomic forces based on structural descriptors extracted from quantum calculations. Several machine-learning frameworks have been developed, including Gaussian approximation potentials (GAP),[23] neural network potentials (NNP),[22] and message-passing neural networks (MPNNs)[25] such as SchNet,[26] MACE (Message Passing Atomic Chemical Environment),[27] and NequIP (Neural Equivariant Interatomic Potentials)[28] enabling them to robustly capture complex bonding environments and chemical transformations, including those in boron and boron compounds. MPNNs, in particular, have shown significant promise due to their improved transferability over diverse bonding environments as compared to traditional methods.[27,29] These frameworks have been trained on vast sets of structure−energy data derived from quantum-level calculations, yielding near-universal foundational models that cover most of the periodic table. The PFP (Preferred Potential)[30] implemented in Matlantis[31] is a proprietary MLIP framework and foundational model that has shown superior performance across a wide range of chemical environments.[32] Another recently emerging MLIP model is SevenNet,[33] which is based on the NequIP[28] MPNN framework. Among the models evaluated for performance in predicting structures and energies of inorganic crystals by Matbench Discovery,[34] SevenNet-MF-ompa is currently one of the best (second place in root-mean-square deviation of atomic

https://doi.org/10.1021/acs.jpcc.5c04822
J. Phys. Chem. C 2025, 129, 22319−22333

coordinates). Here, we compare the predictions of these MLIPs to ReaxFF parameter sets and reference DFT calculations.

The structural diversity of boron clusters has been a subject of significant interest for several decades. Theoretical investigations by Boustani[11] predicted that boron atoms can assemble into stable planar or quasi-planar geometries (borophenes). Studies on clusters such as the B_{40}^- ion provided early evidence that boron could form hollow,[35] fullerene-like cages with bonding characteristics distinct from those found in carbon fullerenes. Building on this foundation, later theoretical work predicted the existence of even larger boron fullerenes. Among these, the B_{80} buckyball was initially proposed by Gonzalez Szwacki et al.[36] using density functional theory (DFT) as a boron analog of the C_{60} fullerene. This structure, shown in Figure 1A, has a form similar to C_{60} (a truncated icosahedron), but with an additional boron atom placed at the center of each of the 20 hexagons. Prasad and et al.[37] showed that "stuffing" the B_{80} buckyball framework with extra boron atoms yields clusters (e.g., B_{98}, B_{100}) that are more stable than the original B_{80} fullerene. In addition to clusters of icosahedral symmetry, Hayami et al.[12] studied a range of boron clusters with octahedral and tetrahedral symmetries.

It should be noted that the term "icosahedral" is used in in two different senses in this work. First, we refer to materials including B_{12} icosahedra as "icosahedral boron materials", although unit cells of these materials do not (and cannot) have overall icosahedral symmetry. Second, we also describe clusters with icosahedral symmetry, such as the B_{80} buckyball, that do not include B_{12} icosahedra.

No evidence of the B_{80} buckyball surfaced in experiments,[38,39] and subsequent DFT studies revealed that the B_{80} buckyball is not the lowest-energy isomer.[40,41] Instead, Zhao et al. 2010[40] and Li et at. 2010[41] discovered that core−shell structures comprising a B_{12} icosahedral core surrounded by roughly hemispherical cages are of significantly lower energy. The core−shell of Zhao et al. is shown in Figure 1B. Subsequently, De et al.[42] found a similar B_{80} core−shell structure (Figure 1C) by minima hopping global geometry optimization that was even lower energy (≈1 eV less) and may represent the thermodynamically favored form of B_{80} at low and ambient temperatures. Both of these core−shell structures have no overall symmetry and exhibit a variety of local bonding networks, with coordination numbers of 6−8 in the core and 4−7 in the shell.

A prerequisite for realistic modeling of icosahedral boron compounds is an accurate representation of the icosahedral motif, which is present in elemental boron and some small pure boron clusters, including the lowest energy core−shell structures.[13] With the goal of simulating synthesis of boron suboxide (B_6O), we developed a set of B/O/Ni ReaxFF parameters. However, we quickly found discrepancies for small boron clusters and boron interfaces, whose realistic representation would be necessary for simulating synthesis of icosahedral boron materials. We also found that the existing "B/N/Ni" parameter set of Liu et al.[43] apparently did no better for pure boron clusters. After discovering this, we decided to focus mostly on the boron force field alone, and leave its interaction with oxygen (and, thus, the representation of boron suboxide) to future work.

Therefore, we generated two new versions of the ReaxFF parameters, adding new structures to the training set, including the B_{80} buckyball of Gonzalez Szwacki et al.[36] (Figure 1A), the Zhao et al. 2010[40] B_{80} core−shell (Figure 1B), and a dubious B_{80} structure generated in our simulations (Figure 1C), which we denote as the "Pouch". These versions (Versions 2 and 3) gave increasingly improved agreement for the relative energies of the three training structures compared to DFT. Furthermore, we evaluated the force fields with test set of 58 additional structures consisting of 8−103 boron atoms. We also conducted larger scale simulations of boron crystallization from a supercooled melt, finding greater production of icosahedron-like motifs in Version 3 compared to previous versions and the B/N/Ni ReaxFF parameter set.[43] We tested the behavior of all four parameter sets for crystal growth under a variety of conditions, including different temperatures, pressures, and in the presence and absence of various seed crystals.

MATERIALS AND METHODS

Density Functional Theory for Training Set. Density functional theory (DFT) was employed to generate training set data for B/O/Ni systems, in line with our initial goal of simulating boron suboxide (although we have chosen to focus on pure boron here). The Version 1 ReaxFF parameters were optimized to match the DFT-derived lattice constants, charges, formation energies, and equations of state for a set of ideal and defective crystals. Table S1 of the Supporting Information (SI) summarizes the composition of the training data set initially used for ReaxFF parameter training, which included several boron allotropes, boron oxides of varying stoichiometries, boron suboxide (B_6O) with defects, and various nickel borides and oxides. Their initial structures were obtained from the Materials Project.[7] Subsequent versions (Versions 2 and 3) included B_{80} clusters as well, which were obtained from Li et al.[13] or ReaxFF simulations with Version 1 (the "Pouch").

Training set DFT calculations performed with periodic boundary conditions using the Vienna Ab Initio Simulation Package (VASP),[44] employing the projector augmented wave (PAW) method[45] to treat the core electrons. The plane wave basis set was expanded with an energy cutoff up to 520 eV. The generalized gradient approximation Perdew−Burke−Ernzerhof (GGA-PBE) functional[46] was used to account for the electronic exchange and correlation effects. The tetrahedron method with Bloch correction was used to determine the partial occupancy of each orbital with the width of smearing as 0.05. For systems containing Ni, calculations were run with a spin-polarized setting. Bulk structures were optimized by allowing the primitive cell atoms to relax within a fixed unit cell boundary. The break conditions are 1×10^{-6} for electronic self-consistent iterations, and −0.02 eV· Å for ionic relaxations, respectively. The automatically generated Γ-centered *k*-point meshes were used with the *k*-point density of 0.3 per Brillouin zone volume.

For calculations involving isolated boron clusters, the clusters were placed in boxes with dimensions of $20 \times 20 \times 20$ Å^3, significantly larger than the clusters themselves. The cutoff energy was set to 520 eV, and the convergence criteria remained unchanged. However, for these nonperiodic systems, a single Γ-point was used for *k*-point sampling. Relaxation of the DFT-derived B_{80} structures taken from Li et al.[13] yielded little change in the coordinates, with RMSD values of <0.01 Å between the initial and final relaxed structures. In contrast, relaxation of the Pouch structure derived from our Version 1 ReaxFF parameters induced a relatively large change of 0.65 Å, highlighting the spurious nature of this structure.

Density Functional Theory for the Test Set. For comparison, DFT calculations were performed using Grid-Based Projector-Augmented Waves (GPAW)[47−49] with the Perdew−Burke−Ernzerhof (PBE) exchange-correlation func-

https://doi.org/10.1021/acs.jpcc.5c04822
J. Phys. Chem. C 2025, 129, 22319−22333

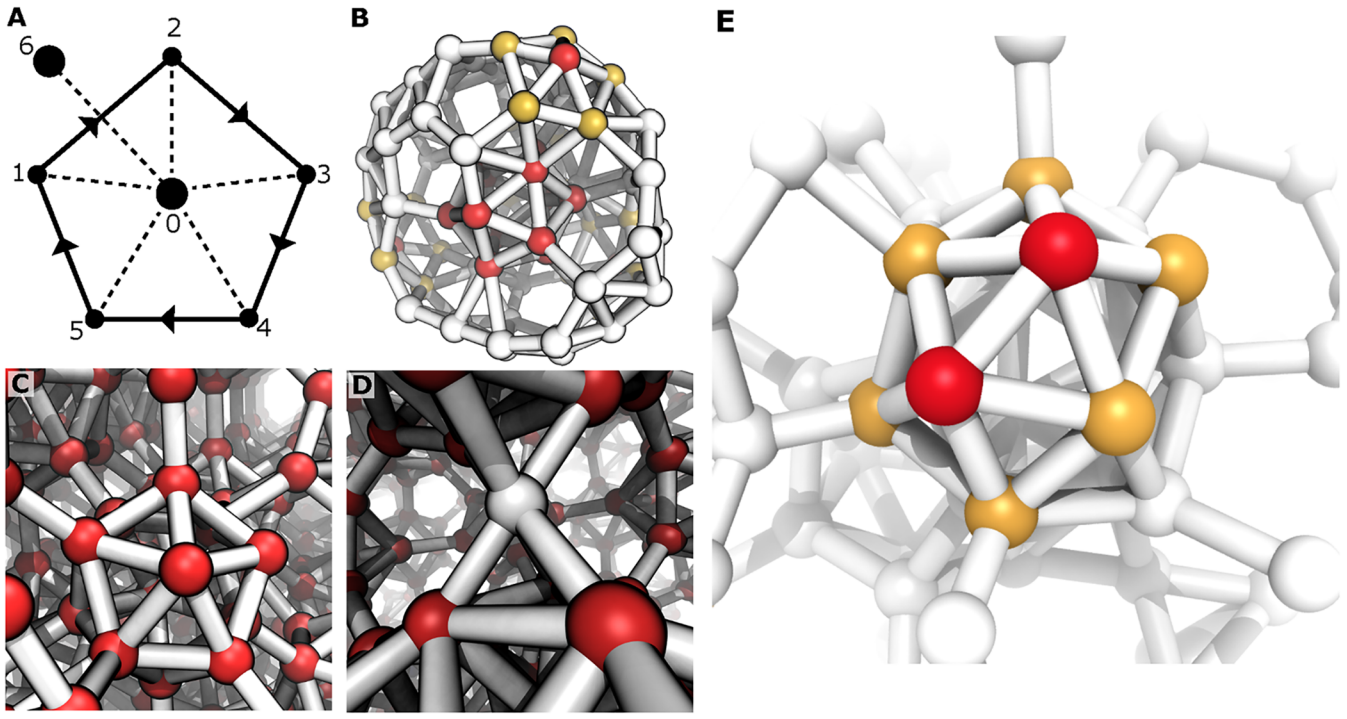

Figure 2. Illustration of the algorithm used to identify icosahedron-like motifs in boron structures and its results. (A) Schematic of the geometry used to identify icosahedral boron atoms. The atoms 1−5 form a pentacycle around the central atom (atom 0). Atom 6 is a boron atom bonded to the central atom 0, but is not part of the pentacycle and exterior to this icosahedral motif (although it may belong to another). (B) The B_{80} core−shell of Li et al.[13] structure marked by our algorithm. Atoms considered by the algorithm to be icosahedral atoms are colored red (and are counted when calculating the quantity "icosahedrality"), while atoms identified by the algorithm as pentacycles around these icosahedral nodes, but not icosahedral nodes themselves, are colored gold. White atoms are not considered to have an icosahedral structure. (C) and (D) show sections of α- and β-rhombohedral boron crystals, respectively, colored according to the same scheme. (E) A partially icosahedral motif that formed in a simulation at 1600 K.

tional.[50] Each cluster's initial atomic coordinates were imported from using the ASE Python library,[51,52] and the structures were centered in simulation cells of dimensions 20 × 20 × 20 Å textsuperscript3, providing a vacuum padding of 10.0 Å around each structure to minimize periodic image interactions.

Calculations employed a plane-wave cutoff energy of 520 eV, and the Brillouin zone was sampled at the Γ-point only. Electron occupations were modeled using Fermi−Dirac smearing with a width of 0.2 eV. The self-consistent field (SCF) convergence criterion for the total energy was set to 1×10^{-5} eV. Structural optimization was carried out using the Broyden-Fletcher-Goldfarb-Shanno (BFGS) algorithm[53] with a force convergence threshold of 0.02 eV/Å.

Molecular Dynamics. We employed the Large-scale Atomic Molecular Massively Parallel Simulator (LAMMPS; Version 23 Jun 2022) to perform reactive molecular dynamics (MD) simulations.[54,55] These simulations were conducted using the ReaxFF framework[17] as implemented in LAMMPS, with GPU-accelerated routines.[56,57] The integration time step was 0.25 fs. Simulations of isolated clusters were performed at constant volume and constant temperature (NVT) conditions, with the temperature controlled via a Langevin thermostat (200 ps damping period). Simulations of continuous boron melts and crystals were performed in the isothermal−isobaric ensemble (NPT), with the temperature and pressure maintained using the Nosé−Hoover thermostat and barostat (time constant, 100 fs). The trajectory was saved in DCD format every 1000 steps. Energy minimization was performed using the conjugate gradient (CG) algorithm.[58] The force tolerance[59] was set to 1.0×10^{-8} kcal·mol^{-1}·Å^{-1}. We utilized the software Visual Molecular Dynamics (VMD)[60] to visualize the trajectories generated by our simulations and associated Tachyon ray tracing engine to generate images.[61] Analysis was performed in VMD using in-house Tcl scripts, which are included in the Zenodo repository associated with this paper.

Energies of Boron Clusters. The DFT-generated structures were obtained from the Supporting Information of the Li et al. article[13] or directly from the authors.[12] The "Pouch" structure was obtained in ReaxFF simulations with Version 1, running at 500 K for 21 ns. All structures are included in the Zenodo repository associated with this work.

As is commonly done for comparisons between different levels of theory,[13,62,63] the energy values were calculated with each ReaxFF parameter set after performing geometry optimization (energy minimization) under that parameter set. This geometry optimization leads to more robust interpretation because the minima of energy basins are compared rather than single-point energies of incompatible sets of coordinates. Comparison of the optimized structures was justified because, as shown in Table 2, each ReaxFF-minimized geometry deviated only slightly from its initial geometry (RMSD < 0.29 Å), indicating that they represent the "same" structure. Furthermore, geometry optimization with the ReaxFF parameter sets did not change the bond network (bond length <2.1 Å). The only exception was the "Pouch" structure derived from our Version 1 ReaxFF parameters, which was altered more substantially by geometry optimization under DFT, with RMSD = 0.67 Å, 26 bonds broken, and 4 new bonds formed. This is described in more detail in the subsection "The "Pouch" Structure" below.

https://doi.org/10.1021/acs.jpcc.5c04822
J. Phys. Chem. C 2025, 129, 22319−22333

Simulation of Growth from a Seed Crystal. In this part of the study, we performed simulations of a boron melt surrounding a small seed crystal under varying pressures and temperatures to gauge the ability of the ReaxFF force fields to represent the growth of icosahedral boron crystals. First, we began with a supercell of the β-rhombohedral (β-B) boron structure containing 1260 atoms. A seed of 236 atoms (≈19% of the total system) was restrained within the initial structure using a force constant of 500 kcal/(mol Å^2). While these atoms were restrained, the system was simulated at 3600 K for 5 ps to ensure that the unrestrained parts of the systems were fully melted. We then used the final configuration from this 3600 K simulation as a starting point for simulations at 1300, 1400, 1500, 1600, and 1700 K and 1 atm of pressure, which were run for 10−30 ns of simulated time. As these temperatures are below the melting point of boron (2348 K), the systems were initially supercooled liquids.[64,65] Experimentally, icosahedral boron compounds such as boron suboxide have been crystallized under high pressure (4−10 GPa),[66,67] so we also performed similar simulations at 10 and 24 GPa. Additionally, we created a larger β-B supercell of 10 080 atoms with a seed of 532 atoms restrained (≈5%). It was melted at 3600 K and then subjected to simulations at various temperatures following the same protocol as above.

Identification of Icosahedrally Coordinated Boron Atoms. To quantify the amount of icosahedral structure formed as the simulation progressed, we developed a set of dependent criteria to identify icosahedrally coordinated boron atoms from a set of atomic coordinates. First, we searched for nearly equilateral triangles involving the central atom and its nearest neighbors. Periodic boundary conditions were accounted for in calculating interatomic distances and angles by using the minimum distance periodic image. Next, we determined whether any of the outer edges of these triangles (those not involving the central atom) formed a 5-membered ring. Finally, for any such rings, we checked how close these 5 atoms are to being coplanar, and ensured the central atom was sufficiently far from this plane. The details of the application of these criteria are given below.

1. **Neighbor Identification.** For each boron atom i not part of the restrained seed, we first identified all atoms within a radial cutoff of 2.1 Å using the `mdtraj` package.[68]
2. **Screening of Neighbor Triangles.** An ideal icosahedron consists of equilateral triangles, with 5 meeting at each vertex. Hence, our algorithm attempted to identify equilateral triangles in the neighborhood of the central atom. Among the nearest neighbors of i, we measured all angles of the form $j-i-k$. If the measured angle deviated by less than ±20° from 60°, we considered those two neighbors (j and k) to form an edge possibly consistent with an icosahedral motif. This step generated an "angle pairs" (j, k) list, capturing potential approximately equilateral triangles with i as the central vertex. If the number of approximately equilateral triangles is less than 5, the algorithm stops, and the atom is not considered icosahedrally coordinated.
3. **Pentacycle Detection.** In icosahedral boron motifs, icosahedrally coordinated boron atoms are surrounded by a pentagon of atoms forming part of an icosahedron (atoms 1−5 in Figure 2A) and typically bonded to 1−3 other boron atoms outside of the nearest icosahedron (atom 6 in Figure 2A). Hence, the algorithm checked all possible five-membered rings (pentacycles) involving the approximately equilateral neighbors identified above. Specifically, we took every combination of five edges from the angle pairs list and constructed an undirected graph. Then, we applied a depth-first search[69] to check whether these edges form a unique cycle of exactly five atoms (Figure 2A). Any such cycle was flagged as a potential set of five faces of an icosahedral fragment. If there were no complete pentacycles in the angle pairs list, the algorithm stopped, and the atom was not considered icosahedrally coordinated.
4. **Planarity Criterion.** In an ideal icosahedron, each vertex is coordinated by 5 adjacent vertices that lie in the same plane, although in practice they are (almost surely) never exactly coplanar. Hence, for each pentacycle identified above, we calculated the best fit plane using principal component analysis (PCA). This plane was defined by the centroid of the 5 pentacycle atoms and a normal vector corresponding to the third principal axis. The pentacycle was considered roughly planar if the root-mean-square deviation of the pentacycle atoms from their best fit plane was less than 0.099 Å.
5. **Central Apex Criterion.** We additionally verified that the distance of the central atom from the best fit plane of the pentacycle exceeded a prescribed cutoff (0.4 Å), since the central atom in an icosahedral motif (index 0 in Figure 2A) should not be in the same plane as the surrounding pentacycle (atoms 1−5).
6. **Calculating the "Icosahedrality".** If at least one pentacycle met both the planarity and central apex criteria, the center atom i was counted as an "icosahedral node". In Figure 2B−E such atoms are marked in red, while atoms in valid pentacycles, but not identified as icosahedral centers themselves, are marked in gold. This algorithm was applied to each frame of the trajectory. Because we are interested in the growth of icosahedral structure from an initial crystal seed, the restrained seed atoms were excluded from the analysis. Hence, the quantity we call "icosahedrality" was calculated as Icosahedrality = $N_{\mathrm{melt}}^{\mathrm{icosa}}/N_{\mathrm{melt}}$, where $N_{\mathrm{melt}}^{\mathrm{icosa}}$ is the number of atoms of the melt identified as an icosahedrally coordinated node by the above algorithm and N_{melt} is the total number of boron atoms in the melt. The restrained seed crystal was not considered part of the melt.

This algorithm gives an icosahedrality of exactly one for ideal α-B crystals (Figure 2C), while giving a value of 312/315 ≈ 0.9905 for β-B crystals due to the presence of 6-coordinate linking atoms in this structure that unambiguously lack icosahedral geometry (Figure 2D). The algorithm marks 16 atoms as icosahedrally coordinated in the Li et al. B_{80} core−shell, including all 12 atoms of the B_{12} icosahedral core and 4 others on the shell (Figure 2B). Hence, our approach captures local geometric features consistent with B_{12} icosahedra. By applying this procedure to each frame of the MD simulations, we obtain a dynamic view of how the icosahedral units emerge and evolve under various thermodynamic conditions and parameter sets. Figure 2E shows a boron motif that emerged from our simulations having several icosahedrally coordinated atoms.

Boron Solubility in Nickel. The solubility of boron in nickel was considered for applications in boron nitride synthesis from liquid metal solutions.[70−72] We constructed a system containing an orthogonal periodic block of α-rhombohedral boron (25.1 × 29.4 × 25.46 Å^3). Free surfaces were made along

https://doi.org/10.1021/acs.jpcc.5c04822
J. Phys. Chem. C 2025, 129, 22319−22333

the z-axis by placing this crystal in a periodic cell with dimensions of 25.1 × 29.4 × 310 Å^3. An face-centered cubic slab of nickel was placed on top of this with (111) surfaces along the z axis (although the initial structure is mostly irrelevant since the crystal quickly melted in the simulations). Unlike the boron crystal, this nickel crystal was not periodic in the xy plane, owing to the incommensurate lattice constants of the two crystals; however, all simulations were performed above the melting point of nickel, so it was able to quickly form a continuous periodic liquid nickel slab in the xy plane. The simulation was performed in the canonical ensemble (NVT) as described above. To estimate the solubilty, we calculated the atom fraction of boron in a region near the center-of-mass of the nickel slab, $|z - z_{\mathrm{COM}}^{\mathrm{Ni}}| < 5$ Å, as a function of simulated time.

RESULTS AND DISCUSSION

The Version 1 Parameter Set. Because our initial goal was to simulate synthesis of boron suboxide (B_6O) from a nickel solution, we trained our first ReaxFF parameter set, denoted Version 1, on crystal structures of elemental boron, boron oxides, nickel oxides, and nickel borides, as well as B_6O structures with defects (Table S1 of the SI), using results from the DFT code VASP.[44] As a first test of this parameter set, we compared its energies and those calculated by DFT for the three B_{80} clusters shown in Figure 1A–C.

As described above, DFT assigns the lowest energy configuration among the B_{80} clusters to the core–shell structure of De et al.[42] (Figure 1C). Therefore, we used energy of this core–shell structure as the reference to compare relative energies. In MD simulations, only relative energies are important, because the time evolution depends only on forces (derivatives of the energy), so it is sufficient to compare $\Delta E = E - E_{\mathrm{De\ core-shell}}$ values. According to our DFT calculations, the B_{80} core–shell of Zhao et al.[40] has an energy $\Delta E = 1.02$ eV above the more optimized core–shell of De et al.[42] This agrees well with Li et al.,[13] who give ΔE values in the range 1.00–1.09 eV using various density functionals (PBE, TPSS, PBE0, and TPSSh). The B_{80} buckyball of Gonzalez Szwacki et al.[36] has an energy somewhat above the Zhao core–shell, with $\Delta E = 2.65$ eV, which is again near the range found by Li et al.,[13] 2.83–4.48 eV.

Table 1 displays the energy values calculated for these B_{80} structures by our Version 1 ReaxFF parameter set. Version 1 gives nearly equal energies for the two core–shell B_{80} structures but reverses their order: it predicts an energy for the Zhao[40] core–shell marginally below that of De[42] ($\Delta E_{\mathrm{Zhao\ core-shell}} = -0.06$ eV, with $\Delta E = E - E(\mathrm{De})$), whereas DFT gives the Zhao core–shell[40] a positive energy relative to that of De.[42] More damningly, Version 1 erroneously predicts the buckyball to have lower energy than either of the core–shells ($\Delta E = -0.51$ eV). Consistent with its favoring of the buckyball structure over the core–shell structure, we find that simulations using Version 1 tend to produce single-shell or borophene-like structures, and disfavor structures including B_{12} icosahedra. One such single-shell structure is considered in the next section. Promisingly, however, energy minimization under Version 1 maintains the structures of all three DFT-derived clusters (Table 2).

Table 1. Relative Energies (eV) of Four B_{80} Structures for the Three ReaxFF Parameter Sets Generated in this Work and DFT[a]

structure	v1	v2	v3	DFT (VASP)	DFT (GPAW)
B_{80} core–shell (De)[42]	0.00	0.00	0.00	0.00	0.00
B_{80} core–shell (Zhao)[40]	−0.06	−0.07	0.91	1.02	1.09
B_{80} buckyball[36]	−0.65	3.07	2.73	2.58	2.76
B_{80} Pouch	−18.04	−0.65	9.96	11.04	11.07

[a]Energies are given relative to geometry-optimized De et al.[42] core-shell (ΔE(structure) = E(structure) − E(De core-shell)). Energies are calculated after geometry optimization under the indicated force field or method, except that single-point calculations were used for the Pouch structure under DFT due to its instability. Except in the latter case, geometry optimization did not alter the bond network and conformational changes were small (see Table 2).

The "Pouch" Structure. To further test the Version 1 parameter set, we performed ReaxFF simulations of the core–shell and buckyball for a range of temperatures. At $T \geq 500$ K, the initial B_{80} buckyball structure evolved into alternative geometries. We chose several low-energy structures from 500 K runs, performed energy minimization on them, and identified a new "Pouch" structure (Figure 1D) that, under Version 1 parameters, had an energy $\Delta E = -18.04$ eV relative to the De et al. core–shell. Despite the Version 1 parmeter set giving such a low energy, this structure is highly disfavored in DFT calculations, having a single-point energy 11.09 eV above De et al. core–shell. Indeed, this structure does not even appear to be metastable under DFT, transforming into a rather different structure (RMSD = 0.67 Å) during DFT geometry optimization. The DFT-relaxed structure has a significantly altered bond network, with 26 of the bonds (bond length <2.1 Å) in the original structure broken and 4 new bonds formed. This suggests that Version 1 parameters may tend to produce structures with overly coordinated boron atoms, as 38 of the 80 boron atoms reduced their coordination number during DFT geometry optimization, reducing the mean coordination number from 6.03 to 5.48. (Table 2)

Table 2. RMSD (Å) from the DFT Reference Structures (or ReaxFF Version 1 Structure for the Pouch) after Energy Minimization Using Three ReaxFF Parameter Sets Developed in this Work

structure	v1	v2	v3
B_{80} core–shell (De)	0.203	0.211	0.206
B_{80} core–shell (Zhao)	0.216	0.193	0.207
B_{80} buckyball	0.186	0.222	0.213
B_{80} Pouch	0.000	0.138	0.145

Refitting ReaxFF Parameters. To correct Version 1's imbalance for boron clusters we added the B_{80} buckyball, Zhao et al. core–shell, and Pouch structures (after DFT geometry optimization) to the training set and refit the ReaxFF parameters, yielding the Version 2 parameter set. As shown in Table 1, Version 2 improves energies of the B_{80} In particular, Version 2 puts the energy of the buckyball above that of the core–shell structures, at $\Delta E = 3.07$ eV, not far from the DFT value. However, while the Pouch is no longer by far the lowest energy of the four structures under Version 2, it still erroneously assigns the Pouch a lower energy than the other B_{80} structures. After investigating the reason for this inadequate improvement, we found that the DFT-relaxed Pouch structure that was added to the training had been substantially altered by geometry optimization, shifting the position of many atoms and changing its bond network, as described in the last subsection. Hence, it was not the original Pouch structure that was penalized in the

https://doi.org/10.1021/acs.jpcc.5c04822
J. Phys. Chem. C 2025, 129, 22319–22333

Table 3. Comparison of Different Force Fields for the Relative Energies of the B_{80} Training Set

structure	B-v3[a]	B/N/Ni[b]	AB[c]	MP-0[d]	MP-0b3[e]	MPA-0[f]	PFP[g]	7Net[h]	DFT[i]
CS (De)	0.00	0.00	0.00	0.00	0.00	0.00	0.00	0.00	0.00
CS (Zhao)	0.91	−3.07	−0.91	0.62	−0.67	0.46	0.91	0.20	1.08
Buckyball	2.73	8.87	−8.44	3.51	−5.98	−3.88	5.11	−0.67	2.75
Pouch	9.96	−20.10	14.76	−0.39	−7.95	−3.41	9.58	0.63	11.07
RMSE[j]	0.65	18.50	6.90	6.65	12.13	9.21	1.61	6.37	0.00

[a]Energies are given relative to those of the De et al.[42] B_{80} core-shell (CS). (a) Boron Version 3 ReaxFF parameter set from this work. [b]B/N/Ni ReaxFF parameter set of Liu et al.[43] [c]Ammonia borane ReaxFF parameter set of Weismiller et al.[73] [d]MACE[27] machine-learning force fields denoted MACE-MP-0. [e]MACE[74] machine-learning force fields denoted MACE-MP-0b3. [f]MACE[75] machine-learning force fields denoted MACE-MPA-0. [g]PFP[30] machine-learning force field (version 7.0.0) executed through Matlantis.[31] [h]SevenNet-MF-ompa.[33] [i]DFT using GPAW[49] (as detailed in Methods). [j]Root-mean-square error relative to DFT reference energies.

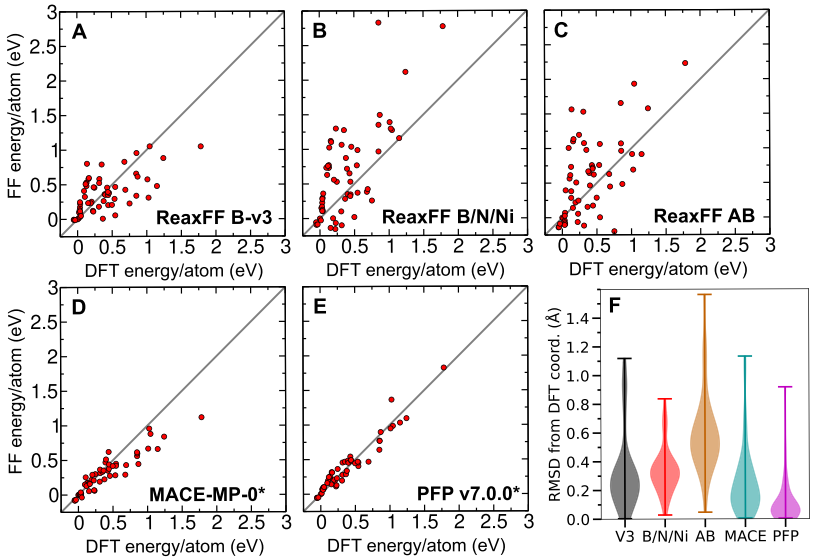

Figure 3. Benchmarking of force fields against DFT for test set of small (8−103 atom) boron clusters. (A−E) Comparison relative energies per atom between DFT and 5 force fields. Per-atom energies are given relative to the per-atom energy of the he De et al. B_{80} core−shell for the same force field/method, and all structures are geometry-optimized under the same force field/method before calculating the energy. (*) For MACE-MP-0 and PFP v7.0.0 there are one and four outlier structures that give results that fall outside of the plots. (F) Violin plot of RMSD values for structures optimized under each force field. DFT-optimized geometries served as the reference structures.

new training set but a distinct structure that represented a local minimum of energy in DFT. As a result, the loss function for Version 2 penalized the energy of the *DFT-relaxed* minimum but left under-penalized the original structure preferred by the Version 1 ReaxFF parameter set. Therefore, we performed a second refinement, using the original Pouch structure and its single-point energy instead of the DFT-relaxed version. This refinement applied the penalty to exactly the geometry where ReaxFF previously produced a spurious minimum. The resulting parameter set, dubbed Version 3 or B-v3, yields much better agreement with DFT (Table 1). It gives the correct ranking for all four of the B_{80} structures shown in Figure 1. Notably, Version 3 strongly disfavors the Pouch relative to the other structures, with ΔE = 9.96 eV, similar to the DFT value of ΔE = 11.09 eV. Furthermore, despite the fact that the De et al. B_{80} core−shell was not included in the training set, Version 3 gives a reasonably accurate difference between the two core−shells (ΔE = 0.91 eV with Version 3 versus 1.02 eV with DFT).

Training Set Performance of Other Force Fields. Our final parameter set (B-v3) is expected to give good agreement in energies for the three B_{80} training set structures (Zhao core−shell, buckyball, and Pouch), since it was specifically optimized for these structures. However, as shown in Table 3, it is illuminating to compare the training set energy values among existing force fields. Here we consider the B/N/Ni ReaxFF parameter set of Liu et al.,[43] the ammonia borane (AB) ReaxFF parameter set of Weismiller et al.,[73] and the universal machine-learning force fields MACE-MP-0, MACE-MP-0b3, MACE-MPA-0,[27,74,75] PFP v7.0.0[30] and SevenNet-MF-ompa.[33] Only B-v3 and PFP yield the correct energy ranking of the training structures. Moreover, B-v3 exhibits the smallest root-mean-square error from the DFT reference (0.65 eV). PFP is the next most accurate, with a root-mean-square error of 1.61 eV, which is mainly due to an overestimation of the energy of the B_{80} buckyball. It seems that the Pouch structure is particularly challenging for empirical force fields, as it causes trouble not only for multiple ReaxFF parameter sets, but also for all three MACE force fields and SevenNet-MF-ompa.[33] Interestingly, newer MACE potentials (MACE-MP-0b3 and MACE-MPA-0) unexpectedly perform worse than the original MACE model trained on Materials Project data (MACE-MP-0). It should be noted that the Pouch structure is considerably altered by energy minimization under the MACE force fields. For example, under MACE-MP-0, the RMSD from the initial structure is 0.79 Å with 37 bonds broken and 16 new bonds formed. However, this does not change the fact that the MACE force fields erroneously predict some kind of single-shell structure to have a lower energy than the lowest energy core−shell structures. Hence, as might be

https://doi.org/10.1021/acs.jpcc.5c04822
J. Phys. Chem. C 2025, 129, 22319−22333

Table 4. Energetic and Structural Accuracy (Relative to DFT) of ReaxFF and Machine-Learning Force Fields for a Test Set of 58 Boron Clusters

structure	B-v3[a]	B/N/Ni[b]	AB[c]	MACE[d]	PFP[e]	SevenNet[f]
Energy correl. r	0.609	0.703	0.607	0.929*	0.820*	0.950*
Energy RMSE (eV/atom)	0.302	0.537	0.489	0.185*	0.238*	0.470*
Energy bias (eV/atom)	−0.013	0.272	0.178	−0.089*	−0.016*	0.346*
RMSD mean (Å)	0.316	0.336	0.589	0.248	0.109	0.170
RMSD median (Å)	0.255	0.316	0.558	0.171	0.070	0.088
RMSD min (Å)	0.003	0.028	0.047	0.005	0.004	0.005
RMSD max (Å)	1.119	0.837	1.563	1.133	0.918	1.396
% RMSD ≤ 0.8 Å	90	98	86	97	98	97
% RMSD ≤ 0.4 Å	86	81	14	86	97	95
% RMSD ≤ 0.2 Å	31	16	2	55	86	74
% RMSD ≤ 0.1 Å	10	3	2	22	72	57

[a]Version 3 ReaxFF parameter set from this work. [b]B/N/Ni ReaxFF parameter set of Liu et al.[43] [c]Ammonia borane ReaxFF parameter set of Weismiller et al.[73]. [d]MACE-MP-0 machine-learning force field.[27,74,75] [e]PFP[30] machine-learning force field (version 7.0.0) executed through Matlantis.[31] [f]SevenNet-MF-ompa.[33] (*) For MACE-MP-0, PFP v7.0.0, and SevenNet-MF-ompa one, three, and one outliers, respectively, with spuriously low relative energies (<−10 eV/atom) were excluded from the energy statistics (but not the RMSD statistics). Raw energy values are given in Tables S3−S5 of the SI.

expected, our ReaxFF B-v3 parameter set performs better than other available force fields for the B_{80} training set, although PFP v7.0.0 does remarkably well considering its general nature.

Boron Cluster Test Set. To validate the final ReaxFF parameter set developed here (Version 3) against DFT data and compare its performance to that of other force fields, we considered a test set of 58 small boron clusters. We included 31 highly symmetric clusters containing 8−100 boron atoms from Hayami et al.,[12] a set of 9 borophene and ring clusters (36−42 atoms) from Pham et al.,[76] and the 18 remaining B_{20}, B_{80}, B_{101}, B_{102}, and B_{103} clusters from Li et al.[13] (excluding the B_{80} core−shell and buckyball used in the training set). In Figure 3A−E, we compare the energies of the energy-minimized structures for 5 force fields, including our B-v3 parameter set, with geometry-optimized DFT references. The statistics of these comparisons are given in Table 4, and the raw energy values are given in Tables S3−S5 of the SI. Of the MACE force fields, we have included only MACE-MP-0, because the statistics for MACE-MP-0b3 and MACE-MPA-0 were worse (lower correlation and higher RMSE).

As shown in Figure 3A−E, all the force fields exhibited moderate correlation with the DFT results in relative per-atom energies. The Pearson correlation coefficient between DFT and each force field varied from $r = 0.950$ for SevenNet-MF-ompa[33] (excluding an absurd outlier, H_B14 of Hayami et al.[12]) to $r = 0.607$ for the ReaxFF ammonia borane force field. Our B-v3 ReaxFF parameter set has among the worst performance for this measure, with $r = 0.609$. However, B-v3 outperformed the other ReaxFF parameter sets in the root-mean-square error (0.3 eV/atom versus ≈0.5 eV/atom), while the B/N/Ni parameter set exhibited the best correlation coefficient ($r = 0.703$) of the three. It is likely that B-v3 would have fared better if this test set had included more asymmetric single-shell structures similar to the Pouch; however, its predictions of energy were reasonably good and, as shown in Figure 3F, it had the best structural accuracy of the ReaxFF parameter sets.

The median RMSD from the DFT-relaxed structure for our B-v3 parameter set was 0.26 Å, handily outperforming the B/N/Ni (0.32 Å) and ammonia borane (0.56 Å) sets. Indeed, RMSD values >0.4 Å are associated with significant changes in the bond network and can hardly be said to maintain the "same" structure. The ammonia borane parameter set showed quite poor structural fidelity, with 14% of structures having RMSD < 0.4 Å and only 2% having RMSD < 0.2 Å. For the B-v3 and B/N/Ni parameter sets, a similar number of structures remained within RMSD < 0.4 Å of the DFT-relaxed structure (86 and 81%). However, B-v3 had nearly twice as many structures with RMSD < 0.2 Å than B/N/Ni (31 versus 16%). For B-v3, 6 structures had RMSD < 0.1 Å, while the other ReaxFF parameters sets had only 2 (B/N/Ni) or 1 (ammonia borane) with such high agreement.

The universal machine-learning interatomic potentials generally performed better for both energy and structure than the ReaxFF potentials, although, in a few cases, they behaved pathologically, yielding dubious structures with B−B bonds <1.42 or even <1.2 Å in length. Being based on chemical bonding theory, ReaxFF is incapable of such extreme pathological behavior. If these outliers had been included in the (nonrobust) energy statistics considered here, MACE-MP-0, PFP v7.0.0, and SevenNet-MF-ompa would have performed worse than all the ReaxFF parameter sets. Both MACE-MP-0 and PFP v7.0.0 showed pathological behavior for the tT_B16 structure of Hayami et al.,[12] with absurdly negative energies of -1.3×10^8 and -1.0×10^3 eV/atom. Interestingly, the newer MACE-MP-0b3 and MACE-MPA-0 force fields do not suffer from this behavior; however, they perform worse overall on the other 57 structures. The tT_B16 structure has 12 boron atoms placed at the vertices of a regular truncated tetrahedron and an 4 additional boron atoms at the center of the 4 hexagonal faces. PFP v7.0.0 also exhibited pathological behavior for the B20_6cs and B20_8s1 structures of Li et al.,[13] with energies of −74 and -9.9×10^2 eV/atom. Another less absurd outlier for PFP v7.0.0 is the T_B20 structure of Hayami et al., which gives an unusually large error in the relative energy for this force field of −1.53 eV/atom. SevenNet-MF-ompa likewise exhibited spurious over-binding for the H_B14 structure of Hayami et al.,[12] yielding −19 eV/atom, which is qualitatively inconsistent with the DFT energy scale for this system. These results suggest that machine-learning potentials still must be used with caution, despite their good accuracy for many cases.

Even including the pathological structures, the machine-learning potentials demonstrated an excellent ability to reproduce DFT-relaxed structures. MACE-MP-0 produced an identical percentage of structures with RMSD < 0.4 Å as our

https://doi.org/10.1021/acs.jpcc.5c04822
J. Phys. Chem. C 2025, 129, 22319−22333

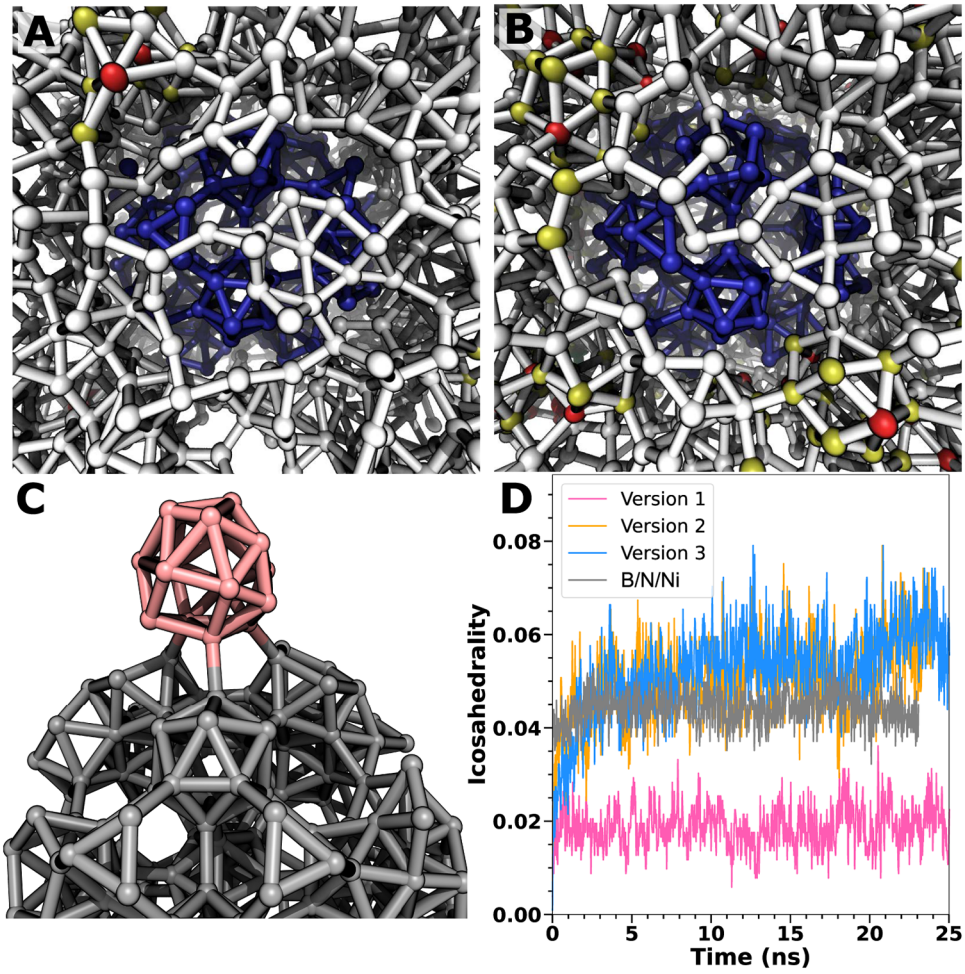

Figure 4. Simulations of structure formation in supercooled liquid boron near a seed crystal. (A) Initial structure for seed simulations. The restrained β-rhombohedral seed region is shown in blue. The supercooled liquid is shown in white, with red indicating icosahedrally coordinated atoms and gold, atoms forming their icosahedral pentacycles. (B) Seed simulation after 10 ns at 1600 K with the Version 3 force field. (C) A B_{17} cluster formed on the seed from initially liquid-phase atoms at 1600 K with the Version 3 force field. (D) Fraction of atoms considered icosahedral as a function of time at 1600 K for four different force fields.

ReaxFF B-v3 (86%), but had more than twice as many structures with RMSD < 0.1 Å (22 versus 10). The structural fidelity of PFP v7.0.0 was remarkable, having 72% of the structures (42 of 58) with RMSD < 0.1 Å. SevenNet-MF-ompa fell between PFP and MACE, with 95% below 0.4 Å (55/58) and 57% below 0.1 Å (33/58).

Crystallization From Seed in Supercooled Melt. To investigate the performance of different versions of ReaxFF parameters during the crystallization of icosahedral boron phases, we conducted a series of simulations aimed at modeling the growth of crystalline boron from small seed crystals at different temperatures. The seed crystal was intended to serve as a nucleation point for the growth of a larger crystal structure as the simulation progresses; however, as shown in the next subsection, icosahedral structure can form spontaneously in the absence of a seed. In the seed growth simulations, the boron system was partitioned into two distinct regions: a restrained region, shown in blue in Figure 4A, which served as the seed crystal; and a supercooled melt region, which was allowed to evolve freely during the simulation. At the beginning of this simulation, almost no icosahedral structure was present in the melt, but as can be seen in Figure 4B, many more icosahedral motifs were present after 10 ns of simulation. Particularly with Versions 2 and 3, we observed spontaneous formation of clusters with icosahedral coordination, although no complete B_{12} icosahedra were formed in any of the simulations. An example of a B_{17} cluster with several icosahedrally coordinated atoms formed in simulations with Version 3 is shown in Figure 4C.

To characterize the evolution of icosahedron-like arrangements, we monitored the *icosahedrality* (see "Identification of Icosahedrally Coordinated Boron Atoms" in Methods) in the supercooled liquid region, which measures the fraction of boron atoms whose local neighborhoods are similar to those in a B_{12} icosahedron. Figure 4D shows this icosahedrality at 1600 K for four different ReaxFF variants: Versions 1, 2, 3, and the previously published "B/N/Ni" force field.[43,72,77] Initially, the supercooled liquid has very low icosahedrality (~0.0150), which rises to varying degrees for each force field, before reaching a plateau. The mean icosahedrality was calculated excluding the first 10 ns to ensure that the reported mean values reflect a steady-state regime. Version 1 shows a small increase in the first hundred picoseconds, but then remains at the same low level over 25 ns of simulation: (1.81 ± 0.45)% (mean ± SD). In contrast, Versions 2 and 3 exhibit a rapid rise above 4% within 1 ns. By 10 ns, Versions 2 and 3 appear to plateau at (5.3 ± 0.8)%. and (5.8 ± 0.8)% (mean ± SD), respectively. The B/N/Ni force

https://doi.org/10.1021/acs.jpcc.5c04822
J. Phys. Chem. C 2025, 129, 22319−22333

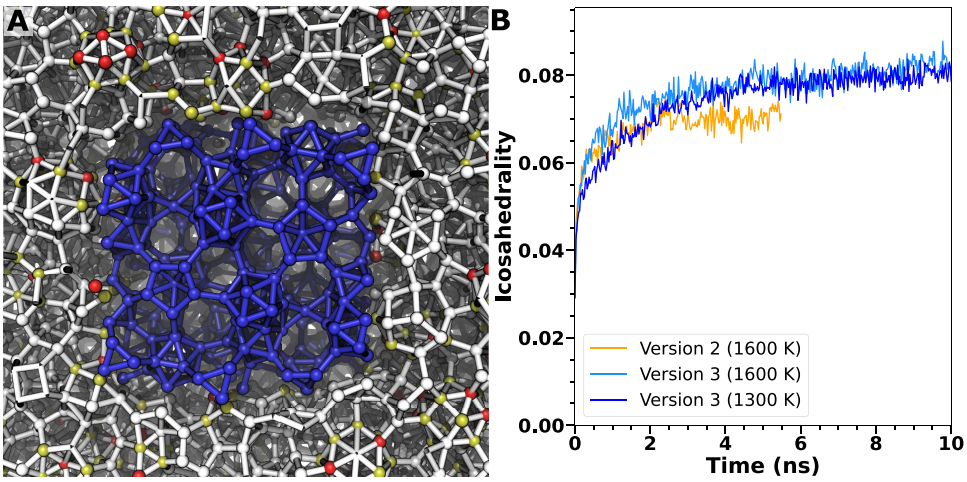

Figure 5. Simulations of structure formation in supercooled liquid boron around a seed crystal for a larger (10,080-atom) system. (A) Initial structure for seed simulations. The same color scheme has been used as described in Figure 4. (A) A cross-section of a seed simulation after 6 ns at 1600 K (Version 3 force field). (B) Fraction of icosahedral structure as a function of time for Version 2 at 1600 K and Version 3 at 1300 and 1600 K.

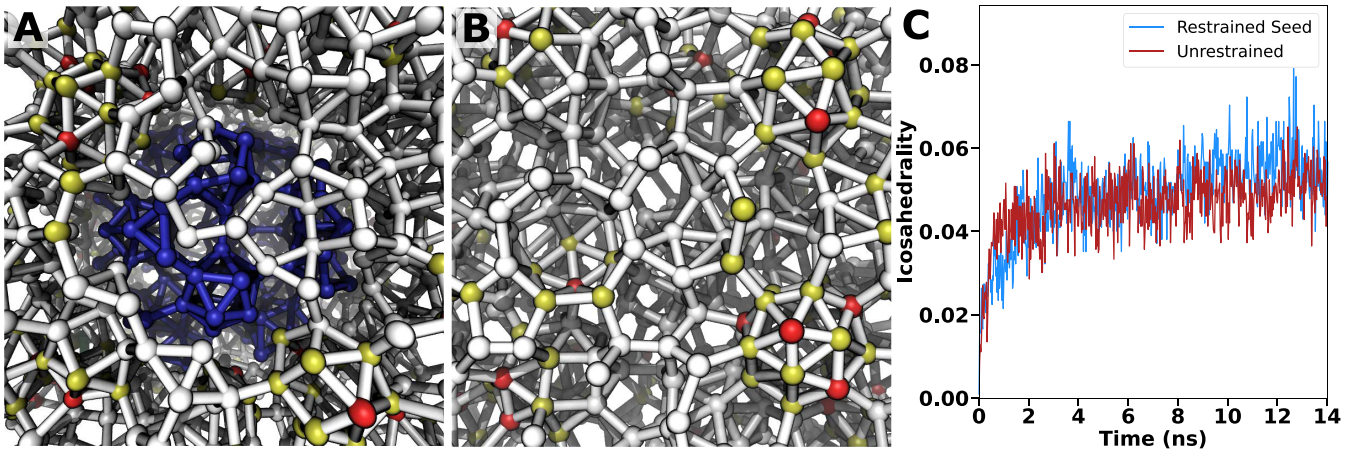

Figure 6. Effect of initial seed on forming icosahedral structure at 1600 K. The same color scheme has been used as described in the caption of Figure 4. Simulations with (A) and without (B) the seed after 14 ns at 1600 K with the Version 3 force field. (C) The icosahedrality at 1600 K for systems with and without the seed.

field exhibits considerably more icosahedral structure than Version 1, but falls below Versions 2 and 3 with (4.4 ± 0.4)% icosahedrality.

For comparison, ideal β- and α-rhombohedral boron phases have icosahedrality values of 99 and 100%. Hence, these simulations have a long way to go to reach full crystallization, if they are even capable of reaching it. An accurate model of boron, in principle, should show the formation of B_{12} and nearly full crystallization if run long enough (seconds or minutes); however, the time scale for crystallization of boron phases are not precisely known and may be longer than the nanosecond time scale accessible to these simulations. Despite this caveat, the results in Figure 4D show the Version 1 force field to be unpromising for simulating crystallization of boron. On the other hand, Versions 2 and 3 appear to be able to model the formation of icosahedron-like structures from supercooled liquid boron. Version 3, in particular, shows the most icosahedral structure of all four force fields. Taken together with the improved agreement with DFT for the energies and structures of small boron clusters, Figure 4D suggests that the refit parameters, particularly Version 3, may yield more accurate models of boron crystallization.

Additional simulations were carried out using a larger system comprising 10 080 atoms to provide increased free space around the seed crystal (Figure 5). In the smaller system discussed earlier, the constrained environment around the seed may restrict the natural growth dynamics; thus, the larger system offers a more realistic setting for nucleation and growth. However, because this system is approximately 8 times larger than the previous one, the simulations for the larger system had to be shorter due to computational constraints. Notably, the tendency of Version 3 to form more icosahedral structure than Version 2 is more pronounced than in the smaller system. Overall, we observe greater formation of icosahedral structure in this larger system, with a mean value approaching 8%. While the formation of icosahedral structure is slower at 1300 K than at 1600 K, as might be expected, the evolution at these two temperatures appears similar $4 < t < 10$ ns. The upward trend in the icosahedrality for Version 3 in the last few nanoseconds suggests that the increase in icosahedrality may continue if the simulation were extended to longer times.

Effect of Seed Crystal on Icosahedral Coordination. To assess the impact of the initial seed on crystallization, we conducted a simulation at 1600 K for the original smaller (1260-

https://doi.org/10.1021/acs.jpcc.5c04822
J. Phys. Chem. C 2025, 129, 22319−22333

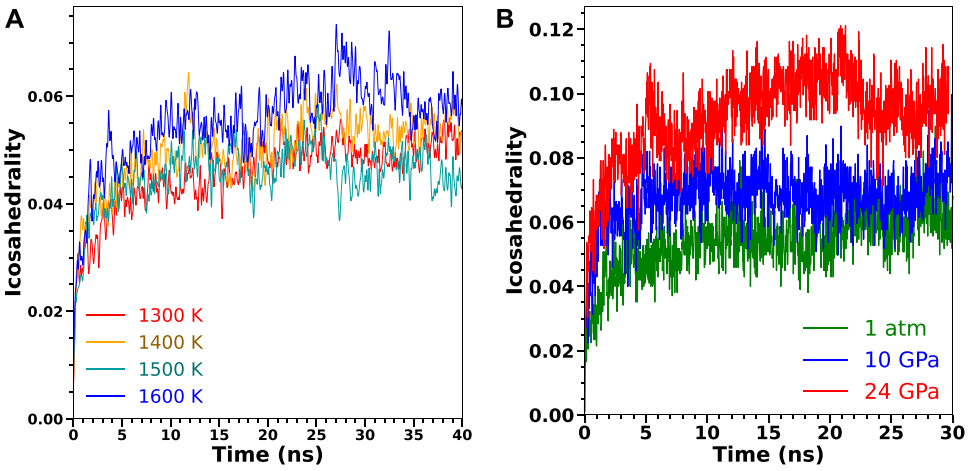

Figure 7. Effect of temperature and pressure on formation of icosahedral structure. (A) Evolution of the fraction of the icosahedral structure during the different simulations at a few selected temperatures. Red, orange, cyan, and blue represent 1300, 1400, 1500, and 1600 K respectively. For clarity, a Gaussian filter was applied to the raw data with a standard deviation of 0.002 ns. (B) The effect of pressure on the formation of the icosahedral configuration during simulations at 1600 K. The red curve corresponds to a pressure of 24 GPa, the blue curve to 10 GPa, and the green curve to 1 atm.

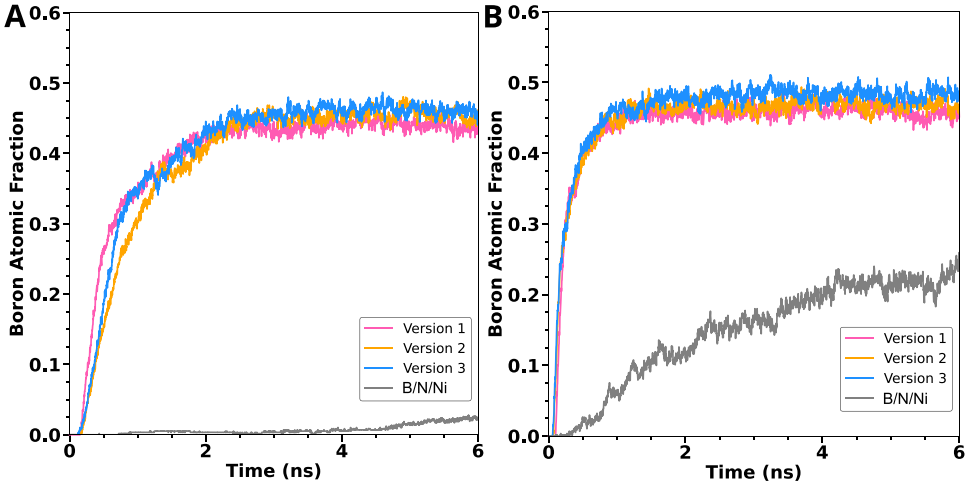

Figure 8. Simulated boron solubility in nickel in the slab center at two temperatures. (A) at 1750 K and (B) at 2000 K comparing the behavior of four different ReaxFF parameter sets: B-v1, B-v2, B-v3, and B/N/Ni.[43]

atom) system without any restrained seed region and compared it to the seeded case. As before in the seed simulations, the boron was melted in a short simulation at 3600 K. In contrast to the previous simulations, no restraints were applied during or after this high-temperature simulation. The temperature was afterward held at 1600 K. As might be expected, the mean proportion of icosahedral structure was less in the absence of the seed than in its presence (Figure 6C): $(4.9 \pm 0.6)\%$ versus $(5.7 \pm 0.8)\%$. However, the difference is not dramatic. We initially performed the simulations including the seed crystal because we thought it would be necessary to accelerate the formation of the icosahedral structure; however, Figure 6 shows that the effect of the restrained seed crystal is modest on the time scale of these simulations and that icosahedral structure can form spontaneously without the presence of a seed. These results indicate spontaneous nucleation remains a viable pathway for icosahedral structure formation under these conditions.

Temperature Dependence of Icosahedral Coordination. We performed similar restrained seed simulations at 1300, 1400, 1500, and 1600 K for the smaller system (Figure 7A) and simulations at 1300 and 1600 K for the larger system (Figure 5B), using the Version 3 force field. For both of these systems, the amount of icosahedral structure did not show any clear trends in the temperature range 1300−1600 K. The mean icosahedrality was near 5% in all cases for the smaller systems. There appear to be differences in the mean icosahedrality near the end of the simulations, but given that the dependence is not monotonic in temperature, it is likely that these differences are not reproducible. Performing replicates with different initial conditions at each temperature could help to distinguish real trends from statistical differences; however, obtaining 40 ns of simulated time requires several months of continuous simulation. For the larger (10K atom system), the icosahedrality plateaus near 8% for both temperatures, with again no clear dependence on temperature.

Pressure Dependence of Icosahedral Coordination. High pressures (several GPa) have often been used to induce formation of high-quality crystals of boron materials.[78,79] In the simulations discussed thus far, we focused on near-atmospheric pressures; here, we increased the pressure to 10 or 24 GPa to investigate whether higher pressure enhances the formation of icosahedral coordination. As shown in Figure 7B, these pressures had a significant effect on the evolution of coordination. At the earliest times ($t < 1$ ns), all three conditions

https://doi.org/10.1021/acs.jpcc.5c04822
J. Phys. Chem. C 2025, 129, 22319−22333

exhibit a relatively low icosahedrality, reflecting liquid-like or amorphous structure. As the simulation proceeds, the icosahedral fraction gradually increases for all pressures, indicative of ongoing local ordering. Notably, the 10 and 24 GPa simulations show a higher icosahedrality than the 1 atm case, suggesting that elevated pressure may indeed promote local clustering of boron into B_{12}-type structures. The most icosahedral structure found in any of our simulations was formed at 24 GPa, with >10% of atoms considered icosahedrally coordinated.

Boron Solubility in Liquid Nickel. Evaluating the developed boron force field requires it to accurately reproduce boron solubility trends in nickel, particularly to accurately model hBN synthesis from molten metals solutions or alloys,[72,77] It is critical that our developed force field (Version 3) reliably reproduces boron solubility trends in liquid nickel. Motivated by these considerations, we evaluated the performance of our refined force field parameters to examine the solubility of boron in nickel under high-temperature conditions, we performed simulations of a Ni block in contact with an α-rhombohedral boron crystal at 1750 and 2000 K using three different ReaxFF parameter sets developed in this study and the previously published B/N/Ni parameter set.[43,72,77] Reference values in the literature provide a context for these results. According to Vitry,[80] one would expect around 62 atom % boron (corresponding to 23 wt %) at 1750 K, with an increase to about 77 atom % boron near 2000 K. On the other hand, studies by Xu and Zhai[81,82] suggest a solubility of 68 atom % boron at 1750 K. The relationship between mass fraction (μ_B) and the atomic fraction (x_B) is given by

$$x_B = \frac{\mu_B}{\mu_B + (1 - \mu_B)M_B/M_{Ni}} \quad (1)$$

where $M_B \approx 10.81$ g/mol and $M_{Ni} \approx 58.69$ g/mol.

In our simulations, solubility was quantified by computing number of boron and nickel atoms residing in the central region of the Ni slab, which was defined as $-5 \leq z - z_{COM} < 5$ Å, where z_{COM} was the center of mass of the slab. Figure 8A shows that the Version 3 force field predicts an average boron fraction of approximately 0.46, while at 2000 K the boron fraction increases to roughly 0.50. This trend is consistent with the expectation that higher temperatures facilitate greater boron dissolution in nickel. For the B/N/Ni force field, dissolution of the α-rhombohedral boron crystal happens more slowly, and it is unclear whether it has reached dynamic equilibrium within the 6 ns of the simulation. However, although the B-v3 force field appears to slightly underestimate the solubility of boron in liquid nickel, it represents a significant improvement over the B/N/Ni force field previous used to study boron in liquid nickel solutions.[72]

CONCLUSIONS

We have developed and validated a new set of ReaxFF parameters (B-v3) that substantially improves the description of boron clusters relative to existing ReaxFF parameter sets. By systematically incorporating both low-energy and high-energy B_{80} isomers, including a dubious B_{80} single-shell ("Pouch") structure discovered in ReaxFF simulations, we achieved a closer agreement in energies with density functional theory (DFT). In particular, of the ReaxFF (our Versions 1−3, B/N/Ni,[43] and ammonia borane[73]) and machine-learning (MACE[75] variants MACE-MP-0, MACE-MP-0b3, and MACE-MPA-0 and PFP v7.0.0[30]) potentials considered, only B-v3 and the proprietary PFP force field correctly ascribe a large relative energy to the difficult Pouch structure. Moreover, only B-v3 reproduces the correct energetic ranking of the B_{80} core−shell, buckyball, and Pouch structures with a root-mean-square error <1 eV. The relative energies of boron clusters vary by 1−2 eV among different quantum mechanical methods;[13,83−85] hence, refining the agreement to better than about 1 eV is probably not worthwhile. This study highlights the importance of including improbable high-energy structures, like the Pouch, in training sets for empirical potentials, in addition to low-energy clusters and crystals.

For a diverse test set of 58 boron clusters, including polyhedral clusters, core−shells, borophenes, and rings, our B-v3 parameter set exhibited the lowest root-mean-square error in relative per-atom energy among the ReaxFF parameter sets. It also best reproduced the DFT-relaxed structures among the ReaxFF potentials, with the lowest mean and median RMSD and with the greatest number of structures with RMSD values below 0.4, 0.2, and 0.1 Å. Although the general machine-learning force fields MACE-MP-0, PFP v7.0.0, and SevenNet-MF-ompa outperformed the ReaxFF potentials in both structure and energy for this test set, in a few cases these force fields produced structures with unrealistically short B−B bond lengths and absurdly negative energies. Hence, while showing great promise, these potentials may need to be used with more caution than ReaxFF, and would probably also benefit from refinement with pathological structures. As shown in Table S9 of the SI, GPU-accelerated simulations with ReaxFF are also several times faster than those with MACE models and require much less onboard GPU memory. Furthermore, the older MACE-MP-0 potential outperformed the newer MACE-MP-0b3 and MACE-MPA-0 potentials (excluding one outlier structure for MACE-MP-0) in relative energies for both the training and test sets, highlighting trade-offs that may come with refinements.

The refinement of the ReaxFF parameters undertaken in this work enhanced the formation of icosahedral motifs during simulations of supercooled boron melts. Using a newly developed algorithm and freely released Python code, we determined the fraction of boron atoms with local coordination similar to B_{12} icosahedra, and found that our B-v3 parameter exhibits greater formation of icosahedral coordination than its earlier iterations (Versions 1 and 2) or the previously published B/N/Ni[43] ReaxFF parameter set. Higher pressures (10−24 GPa) further promoted spontaneous icosahedral ordering, up to >10%; however, the true time scale for nucleation and growth of boron crystals may be longer than the tens of nanoseconds currently accessible to ReaxFF simulations. Finally, our B-v3 parameter set more realistically models boron solubility in nickel than previously available ReaxFF parameters.

While this new parameter set is a substantial improvement for representing boron clusters and icosahedral boron materials with ReaxFF, some residual errors remain between ReaxFF predictions and DFT for boron clusters. The correlation with DFT for relative per-atom energies in the 58-cluster test set was only moderate: $r = 0.61$. Excluding a few absurd outliers, the MACE-MP-0, PFP v7.0.0, and SevenNet-MF-ompa machine-learning potentials did substantially better, with $r = 0.93$, $r = 0.82$, and $r = 0.95$, respectively. It remains unclear whether the B-v3 parameter set, or any existing empirical potential, can exhibit spontaneous crystallization of icosahedral boron materials and whether such crystallization happens on time scales accessible to atomistic simulation.

https://doi.org/10.1021/acs.jpcc.5c04822
J. Phys. Chem. C 2025, 129, 22319−22333

Future work might broaden the training set to include additional boron clusters, allotropes, and compounds, as well transition states and high-energy decoy structures similar to the Pouch. Nonetheless, the B-v3 presented here enables simulation of icosahedral structure formation and high-temperature boron−nickel systems, potentially accelerating the design of new boron-based materials and synthesis methods.

■ ASSOCIATED CONTENT

Data Availability Statement

LAMMPS and GPAW input files, including structure files and configuration files, along with output (LAMMPS log files, LAMMPS restart files, and downsampled DCD-format trajectory files) are freely available for download from Zenodo (https://doi.org/10.5281/zenodo.15858472). We have also included analysis scripts (VMD Tcl or Python) and the processed data produced by these scripts.

Supporting Information

The Supporting Information is available free of charge at https://pubs.acs.org/doi/10.1021/acs.jpcc.5c04822.

The Supporting Information includes supplemental methods, 8 tables of data, and the text of the ReaxFF parameter file for the Version 3 parameter set developed in this work (PDF)

■ AUTHOR INFORMATION

Corresponding Authors

Amin Ahmadisharaf − *Tim Taylor Department of Chemical Engineering, Kansas State University, Manhattan, Kansas 66506, United States;* orcid.org/0009-0003-4680-9905; Email: ahmadish@ksu.edu

Jeffrey Comer − *Department of Anatomy and Physiology, Kansas State University, Manhattan, Kansas 66506, United States;* orcid.org/0000-0003-4437-1260; Email: jeffcomer@ksu.edu

Authors

Adri C. T. van Duin − *Department of Mechanical Engineering, Department of Chemistry, Department of Materials Science and Engineering, Department of Chemical Engineering, Pennsylvania State University, University Park, Pennsylvania 16802, United States;* orcid.org/0000-0002-3478-4945

Bin Liu − *Tim Taylor Department of Chemical Engineering, Kansas State University, Manhattan, Kansas 66506, United States;* orcid.org/0000-0001-7890-7612

Dylan Evans − *Tim Taylor Department of Chemical Engineering, Kansas State University, Manhattan, Kansas 66506, United States*

Sadra Sabouri − *Thomas Lord Department of Computer Science, University of Southern California, Los Angeles, California 90089, United States;* orcid.org/0000-0003-1047-2346

Complete contact information is available at: https://pubs.acs.org/10.1021/acs.jpcc.5c04822

Author Contributions

Amin Ahmadisharaf: "Software", "Investigation", "Visualization", "Writing−original draft". Adri Van Duin: "Methodology", "Software", "Writing−review & "editing". Bin Liu: "Investigation", "Methodology", "Funding acquisition", "Writing" − "review" & "editing". Dylan Evans: "Investigation", "Software", "Writing−review" & "editing". Sadra Sabouri: "Software", "Methodology". Jeffrey Comer: "Conceptualization", "Methodology", "Software", "Investigation", "Funding acquisition", "Supervision", "Visualization", "Writing−original draft", "Writing−review" & "editing.

Notes

The authors declare no competing financial interest.

■ ACKNOWLEDGMENTS

This project was supported by the Department of Energy under grants DE-SC0021264 and DE-SC0026042. A. C. T. v. D. acknowledges funding from AFOSR/MURI project FA9550-24-1-0301 and from ONR/MURI project N000142412313. A majority of the computing for this project was performed on the Beocat Research Cluster at Kansas State University, which is funded in part by NSF grants CHE-1726332, CNS-1006860, EPS-1006860, and EPS-0919443. The authors thank James H. Edgar for his valuable comments.

■ REFERENCES

(1) Fujimori, M.; Nakata, T.; Nakayama, T.; Nishibori, E.; Kimura, K.; Takata, M.; Sakata, M. Peculiar Covalent Bonds in α-rhombohedral Boron. *Phys. Rev. Lett.* **1999**, *82*, 4452.

(2) Frye, C. D.; Edgar, J.; Zhang, Y.; Cooper, K.; Nyakiti, L. O.; Gaskill, D. Synthesis of Icosahedral Boron Arsenide Nanowires for Betavoltaic Applications. *MRS Proc.* **2012**, *1439*, 69−75.

(3) Biffi, M.; Ziacchi, M.; Bertini, M.; Sangiorgi, D.; Corsini, D.; Martignani, C.; Diemberger, I.; Boriani, G. Longevity of Implantable Cardioverter-defibrillators: Implications for Clinical Practice and Health Care Systems. *Europace* **2008**, *10*, 1288−1295.

(4) Hein, F.; Thull, R. *Engineering in Medicine: Vol. 1: Advances in Pacemaker Technology*; Springer Science & Business Media, 2012.

(5) Zarechnaya, E. Y.; Dubrovinsky, L.; Dubrovinskaia, N.; Filinchuk, Y.; Chernyshov, D.; Dmitriev, V.; Miyajima, N.; El Goresy, A.; Braun, H. F.; Van Smaalen, S.; et al. Superhard Semiconducting Optically Transparent High Pressure Phase of Boron. *Phys. Rev. Lett.* **2009**, *102*, No. 185501.

(6) Edgar, J. H.; Hoffman, T. B.; Clubine, B.; Currie, M.; Du, X.; Lin, J.; Jiang, H. Characterization of Bulk Hexagonal Boron Nitride Single Crystals Grown by the Metal Flux Technique. *J. Cryst. Growth* **2014**, *403*, 110−113.

(7) Jain, A.; Ong, S. P.; Hautier, G.; Chen, W.; Richards, W. D.; Dacek, S.; Cholia, S.; Gunter, D.; Skinner, D.; Ceder, G.; Persson, K. A. Commentary: The Materials Project: A Materials Genome Approach to Accelerating Materials Innovation. *APL Materials* **2013**, *1*, No. 011002.

(8) Higashi, I.; Kobayashi, K.; Tanaka, T.; Ishizawa, Y. Structure Refinement of YB_{62} and YB_{56} of the YB_{66}-Type Structure. *J. Solid State Chem.* **1997**, *133*, 16−20.

(9) Ou, M.; Wang, X.; Yu, L.; Liu, C.; Tao, W.; Ji, X.; Mei, L. The Emergence and Evolution of Borophene. *Adv. Sci.* **2021**, *8*, No. 2001801.

(10) Tang, H.; Ismail-Beigi, S. Novel Precursors for Boron Nanotubes: The Competition of Two-Center and Three-Center Bonding in Boron Sheets. *Phys. Rev. Lett.* **2007**, *99*, No. 115501.

(11) Boustani, I. Systematic Ab Initio Investigation of Bare Boron Clusters: Determination of the Geometry and Electronic Structures of B_n (n = 2−14). *Phys. Rev. B* **1997**, *55*, No. 16426.

(12) Hayami, W.; Otani, S. Structural Stability of Boron Clusters with Octahedral and Tetrahedral Symmetries. *J. Phys. Chem. A* **2011**, *115*, 8204−8207.

(13) Li, F.; Jin, P.; Jiang, D.-e.; Wang, L.; Zhang, S. B.; Zhao, J.; Chen, Z. B_{80} and $B_{101-103}$ Clusters: Remarkable Stability of the Core-shell Structures Established by Validated Density Functionals. *J. Chem. Phys.* **2012**, *136*, No. 074302.

(14) Jakse, N.; Pasturel, A. Interplay between the Structure and Dynamics in Liquid and Undercooled Boron: An Ab Initio Molecular Dynamics Simulation Study. *J. Chem. Phys.* **2014**, *141*, No. 234504.

(15) van Duin, A. C. T.; Dasgupta, S.; Lorant, F.; Goddard, W. A. ReaxFF: a Reactive Force Field for Hydrocarbons. *J. Phys. Chem. A* **2001**, *105*, 9396−9409.
(16) Chenoweth, K.; Van Duin, A. C.; Goddard, W. A. ReaxFF Reactive Force Field for Molecular Dynamics Simulations of Hydrocarbon Oxidation. *J. Phys. Chem. A* **2008**, *112*, 1040−1053.
(17) Senftle, T. P.; Hong, S.; Islam, M. M.; Kylasa, S. B.; Zheng, Y.; Shin, Y. K.; Junkermeier, C.; Engel-Herbert, R.; Janik, M. J.; Aktulga, H. M.; et al. The ReaxFF Reactive Force-field: Development, Applications and Future Directions. *npj Comput. Mater.* **2016**, *2*, No. 15011.
(18) Le, M. Q.; Mortazavi, B.; Rabczuk, T. Mechanical Properties of Borophene Films: a Reactive Molecular Dynamics Investigation. *Nanotechnology* **2016**, *27*, No. 445709.
(19) An, Q.; Goddard, W. A., III Atomistic Origin of Brittle Failure of Boron Carbide from Large-scale Reactive Dynamics Simulations: Suggestions Toward Improved Ductility. *Phys. Rev. Lett.* **2015**, *115*, No. 105501.
(20) Hu, X.; Dai, Y.; Li, R.; Shen, H.; He, X. A Molecular Dynamics Study of Interstitial Boron in Diamond. *Phys. B Condens. Matter* **2003**, *327*, 39−42.
(21) Han, S. S.; Kang, J. K.; Lee, H. M.; Van Duin, A. C.; Goddard, W. A., III The Theoretical Study on Interaction of Hydrogen with Single-walled Boron Nitride Nanotubes. I. The Reactive Force Field ReaxFF(HBN) Development. *J. Chem. Phys.* **2005**, *123*, No. 114703, DOI: 10.1063/1.1999628.
(22) Behler, J.; Parrinello, M. Generalized Neural-network Representation of High-dimensional Potential-energy Surfaces. *Phys. Rev. Lett.* **2007**, *98*, No. 146401.
(23) Bartók, A. P.; Payne, M. C.; Kondor, R.; Csányi, G. Gaussian Approximation Potentials: The Accuracy of Quantum Mechanics, without the Electrons. *Phys. Rev. Lett.* **2010**, *104*, No. 136403.
(24) Yang, Y.; Zhang, S.; Ranasinghe, K. D.; Isayev, O.; Roitberg, A. E. Machine Learning of Reactive Potentials. *Annu. Rev. Phys. Chem.* **2024**, *75*, 371−395.
(25) Gilmer, J.; Schoenholz, S. S.; Riley, P. F.; Vinyals, O.; Dahl, G. E. *Machine Learning Meets Quantum Physics*; Springer, 2020; pp 199−214.
(26) Schütt, K.; Kindermans, P.-J.; Sauceda Felix, H. E.; Chmiela, S.; Tkatchenko, A.; Müller, K.-R.SchNet: A Continuous-filter Convolutional Neural Network for Modeling Quantum Interactions. In *Advances in Neural Information Processing Systems*; Curran Associates, Inc., 2017; pp 1−11.
(27) Batatia, I.; Kovacs, D. P.; Simm, G.; Ortner, C.; Csányi, G.MACE: Higher Order Equivariant Message Passing Neural Networks for Fast and Accurate Force Fields. In *Advances in Neural Information Processing Systems*; Curran Associates, Inc., 2022; pp 11423−11436.
(28) Batzner, S.; Musaelian, A.; Sun, L.; Geiger, M.; Mailoa, J. P.; Kornbluth, M.; Molinari, N.; Smidt, T. E.; Kozinsky, B. E(3)-Equivariant Graph Neural Networks for Data-Efficient and Accurate Interatomic Potentials. *Nat. Commun.* **2022**, *13*, No. 2453.
(29) Unke, O. T.; Meuwly, M. PhysNet: A Neural Network for Predicting Energies, Forces, Dipole Moments, and Partial Charges. *J. Chem. Theory Comput.* **2019**, *15*, 3678−3693.
(30) Takamoto, S.; Shinagawa, C.; Motoki, D.; Nakago, K.; Li, W.; Kurata, I.; Watanabe, T.; Yayama, Y.; Iriguchi, H.; Asano, Y.; et al. Towards Universal Neural Network Potential for Material Discovery Applicable to Arbitrary Combination of 45 Elements. *Nat. Commun.* **2022**, *13*, No. 2991.
(31) Matlantis, Software as a Service Style Material Discovery Tool. https://matlantis.com/, Accessed 2025−07−11.
(32) Mine, S.; Toyao, T.; Shimizu, K.-i.; Hinuma, Y. Comparison of Matlantis and VASP Bulk Formation and Surface Energies in Metal Hydrides, Carbides, Nitrides, Oxides, and Sulfides. *Chem. Lett.* **2023**, *52*, 757−759.
(33) Kim, J.; Kim, J.; Kim, J.; Lee, J.; Park, Y.; Kang, Y.; Han, S. Data-Efficient Multifidelity Training for High-Fidelity Machine Learning Interatomic Potentials. *J. Am. Chem. Soc.* **2025**, *147*, 1042−1054.
(34) Riebesell, J.; Goodall, R. E.; Benner, P.; Chiang, Y.; Deng, B.; Ceder, G.; Asta, M.; Lee, A. A.; Jain, A.; Persson, K. A. A Framework to Evaluate Machine Learning Crystal Stability Predictions. *Nat. Mach. Intell.* **2025**, *7*, 836−847.
(35) Zhai, H.-J.; Zhao, Y.-F.; Li, W.-L.; Chen, Q.; Bai, H.; Hu, H.-S.; Piazza, Z. A.; Tian, W.-J.; Lu, H.-G.; Wu, Y.-B.; Mu, Y.-W.; Wei, G.-F.; Liu, Z.-P.; Li, J.; Li, S.-D.; Wang, L.-S. Observation of an All-boron Fullerene. *Nat. Chem.* **2014**, *6*, 727−731.
(36) Gonzalez Szwacki, N.; Sadrzadeh, A.; Yakobson, B. I. B_{80} Fullerene: an Ab Initio Prediction of Geometry, Stability, and Electronic Structure. *Phys. Rev. Lett.* **2007**, *98*, No. 166804.
(37) Prasad, D. L. V. K.; Jemmis, E. D. Stuffing Improves the Stability of Fullerene-like Boron Clusters. *Phys. Rev. Lett.* **2008**, *100*, No. 165504.
(38) Yan, Q.-B.; Zheng, Q.-R.; Su, G. Face-centered-cubic B_{80} Metal: Density Functional Theory Calculations. *Phys. Rev. B* **2008**, *77*, No. 224106.
(39) Sadrzadeh, A.; Pupysheva, O. V.; Singh, A. K.; Yakobson, B. I. The Boron Buckyball and Its Precursors: an Electronic Structure Study. *J. Phys. Chem. A* **2008**, *112*, 13679−13683.
(40) Zhao, J.; Wang, L.; Li, F.; Chen, Z. B_{80} and Other Medium-sized Boron Clusters: Core-shell Structures, Not Hollow Cages. *J. Phys. Chem. A* **2010**, *114*, 9969−9972.
(41) Li, H.; Shao, N.; Shang, B.; Yuan, L.-F.; Yang, J.; Zeng, X. C. Icosahedral B_{12}-containing Core−shell Structures of B_{80}. *Chem. Commun.* **2010**, *46*, 3878−3880.
(42) De, S.; Willand, A.; Amsler, M.; Pochet, P.; Genovese, L.; Goedecker, S. Energy Landscape of Fullerene Materials: a Comparison of Boron to Boron Nitride and Carbon. *Phys. Rev. Lett.* **2011**, *106*, No. 225502.
(43) Liu, S.; Van Duin, A. C.; Van Duin, D. M.; Liu, B.; Edgar, J. H. Atomistic Insights into Nucleation and Formation of Hexagonal Boron Nitride on Nickel from First-principles-based Reactive Molecular Dynamics Simulations. *ACS Nano* **2017**, *11*, 3585−3596.
(44) Kresse, G.; Hafner, J. Ab Initio Molecular Dynamics for Liquid Metals. *Phys. Rev. B* **1993**, *47*, 558.
(45) Kresse, G.; Joubert, D. From Ultrasoft Pseudopotentials to the Projector Augmented-wave Method. *Phys. Rev. B* **1999**, *59*, 1758.
(46) Perdew, J. P.; Burke, K.; Ernzerhof, M. Generalized Gradient Approximation Made Simple. *Phys. Rev. Lett.* **1996**, *77*, 3865.
(47) Mortensen, J. J.; Hansen, L. B.; Jacobsen, K. W. Real-space Grid Implementation of the Projector Augmented Wave Method. *Phys. Rev. B: Condens. Matter Mater. Phys.* **2005**, *71*, No. 035109.
(48) Enkovaara, J.; Rostgaard, C.; Mortensen, J. J.; Chen, J.; Dułak, M.; Ferrighi, L.; Gavnholt, J.; Glinsvad, C.; Haikola, V.; Hansen, H. A.; et al. Electronic Structure Calculations with GPAW: A Real-space Implementation of the Projector Augmented-wave Method. *J. Phys.: Condens. Matter* **2010**, *22*, No. 253202.
(49) Mortensen, J. J.; Larsen, A. H.; Kuisma, M.; Ivanov, A. V.; Taghizadeh, A.; Peterson, A.; Haldar, A.; Dohn, A. O.; Schäfer, C.; Jónsson, E. O.; Hermes, E. D.; Nilsson, F. A.; Kastlunger, G.; Levi, G.; Jónsson, H.; et al. GPAW: An Open Python Package for Electronic Structure Calculations. *J. Chem. Phys.* **2024**, *160*, No. 092503.
(50) Ernzerhof, M.; Scuseria, G. E. Assessment of the Perdew-Burke-Ernzerhof Exchange-correlation Functional. *J. Chem. Phys.* **1999**, *110*, 5029−5036.
(51) Larsen, A. H.; Mortensen, J. J.; Blomqvist, J.; Castelli, I. E.; Christensen, R.; Dułak, M.; Friis, J.; Groves, M. N.; Hammer, B.; Hargus, C.; Jennings, E. D. H. P. C.; Jensen, P. B.; Kermode, J.; Kitchin, J. R.; Kolsbjerg, E. L.; Kubal, J.; Kaasbjerg, K.; Lysgaard, S.; Maronsson, J. B.; Maxson, T.; Olsen, T.; Pastewka, L.; Peterson, A.; Rostgaard, C.; Schiøtz, J.; Schütt, O.; Strange, M.; Thygesen, K. S.; Vegge, T.; Vilhelmsen, L.; Walter, M.; Zeng, Z. The Atomic Simulation Environment-a Python Library for Working with Atoms. *J. Phys.: Condens. Matter* **2017**, *29*, No. 273002, DOI: 10.1088/1361-648X/aa680e.
(52) Bahn, S. R.; Jacobsen, K. W. An Object-oriented Scripting Interface to a Legacy Electronic Structure Code. *Comput. Sci. Eng.* **2002**, *4*, 56−66.
(53) Head, J. D.; Zerner, M. C. A Broyden−Fletcher−Goldfarb−Shanno Optimization Procedure for Molecular Geometries. *Chem. Phys. Lett.* **1985**, *122*, 264−270.

(54) Thompson, A. P.; Aktulga, H. M.; Berger, R.; Bolintineanu, D. S.; Brown, W. M.; Crozier, P. S.; in 't Veld, P. J.; Kohlmeyer, A.; Moore, S. G.; Nguyen, T. D.; Shan, R.; Stevens, M. J.; Tranchida, J.; Trott, C.; Plimpton, S. J. LAMMPS-A Flexible Simulation Tool for Particle-based Materials Modeling at the Atomic, Meso, and Continuum Scales. *Comput. Phys. Commun.* **2022**, *271*, No. 108171.
(55) Plimpton, S. Fast Parallel Algorithms for Short-range Molecular Dynamics. *J. Comput. Phys.* **1995**, *117*, 1−19.
(56) Aktulga, H. M.; Fogarty, J. C.; Pandit, S. A.; Grama, A. Y. Parallel Reactive Molecular Dynamics: Numerical Methods and Algorithmic Techniques. *Parallel Comput.* **2012**, *38*, 245−259.
(57) Carter Edwards, H.; Trott, C. R.; Sunderland, D. Kokkos: Enabling manycore performance portability through polymorphic memory access patterns. *J. Parallel Distr. Compt.* **2014**, *74*, 3202−3216. Domain-Specific Languages and High-Level Frameworks for High-Performance Computing
(58) Fletcher, R.; Reeves, C. M. Function Minimization by Conjugate Gradients. *Comput. J.* **1964**, *7*, 149−154.
(59) Kresse, G.; Furthmüller, J. Efficiency of Ab-initio Total Energy Calculations for Metals and Semiconductors Using a Plane-wave Basis Set. *Comput. Mater. Sci.* **1996**, *6*, 15−50.
(60) Humphrey, W.; Dalke, A.; Schulten, K. VMD − Visual Molecular Dynamics. *J. Mol. Graphics* **1996**, *14*, 33−38.
(61) Stone, J. An Efficient Library for Parallel Ray Tracing and Animation. M.Sc. thesis, Computer Science Department, University of Missouri-Rolla, 1998.
(62) Paupitz, R.; Junkermeier, C. E.; van Duin, A. C.; Branicio, P. S. Fullerenes Generated from Porous Structures. *Phys. Chem. Chem. Phys.* **2014**, *16*, 25515−25522.
(63) Moqadam, M.; Riccardi, E.; Trinh, T. T.; Åstrand, P.-O.; van Erp, T. S. A Test on Reactive Force Fields for the Study of Silica Dimerization Reactions. *J. Chem. Phys.* **2015**, *143*, No. 184113.
(64) Kelton, K. F.; Greer, A. L. *Nucleation in Condensed Matter: Applications in Materials and Biology*; Elsevier, 2010; Vol. *15*.
(65) Ediger, M. D.; Angell, C. A.; Nagel, S. R. Supercooled Liquids and Glasses. *J. Phys. Chem. A* **1996**, *100*, 13200−13212.
(66) McMillan, P. F.; Hubert, H.; Chizmeshya, A. Growth of Icosahedral Boron-rich Clusters at High Pressure. *MRS Proc.* **1997**, *499*, 453−459.
(67) Gladkaya, I.; Dyuzheva, T.; Ekimov, E.; Nikolaev, N.; Bendeliani, N. Crystal Growth at High Pressure and the Problem of Characterization of the Interstitial Phases in the B-C-O System. *J. Alloys Compd.* **2001**, *329*, 153−156.
(68) McGibbon, R. T.; Beauchamp, K. A.; Harrigan, M. P.; Klein, C.; Swails, J. M.; Hernández, C. X.; Schwantes, C. R.; Wang, L.-P.; Lane, T. J.; Pande, V. S. MDTraj: A Modern Open Library for the Analysis of Molecular Dynamics Trajectories. *Biophys. J.* **2015**, *109*, 1528−1532.
(69) Tarjan, R. Depth-first Search and Linear Graph Algorithms. *SIAM J. Comput.* **1972**, *1*, 146−160.
(70) Kubota, Y.; Watanabe, K.; Tsuda, O.; Taniguchi, T. Deep Ultraviolet Light-emitting Hexagonal Boron Nitride Synthesized at Atmospheric Pressure. *Science* **2007**, *317*, 932−934.
(71) Hoffman, T. B.; Clubine, B.; Zhang, Y.; Snow, K.; Edgar, J. H. Optimization of Ni-Cr Flux Growth for Hexagonal Boron Nitride Single Crystals. *J. Cryst. Growth* **2014**, *393*, 114−118.
(72) Ahmadisharaf, A.; Liu, B.; Edgar, J. H.; Comer, J. Growth of Hexagonal Boron Nitride from Molten Nickel Solutions: A Reactive Molecular Dynamics Study. *ACS Appl. Mater. Interfaces* **2025**, *17*, 11213−11226.
(73) Weismiller, M. R.; Van Duin, A. C.; Lee, J.; Yetter, R. A. ReaxFF Reactive Force Field Development and Applications for Molecular Dynamics Simulations of Ammonia Borane Dehydrogenation and Combustion. *J. Phys. Chem. A* **2010**, *114*, 5485−5492.
(74) Kovács, D. P.; Batatia, I.; Arany, E. S.; Csányi, G. Evaluation of the MACE Force Field Architecture: From Medicinal Chemistry to Materials Science. *J. Chem. Phys.* **2023**, *159*, No. 044118.
(75) Batatia, I.; Benner, P.; Chiang, Y.; Elena, A. M.; Kovács, D. P.; Riebesell, J.; Advincula, X. R.; Asta, M.; Avaylon, M.; Baldwin, W. J.et al.A Foundation Model for Atomistic Materials Chemistry. *arXiv* preprint arXiv:2401.00096, 2024.
(76) Pham, H. T.; Duong, L.; Tam, N. M.; Pham-Ho, M.; Nguyen, M. T. The Boron Conundrum: Bonding in the Bowl B_{30} and B_{36}, Fullerene B_{40} and Triple Ring B_{42} Clusters. *Chem. Phys. Lett.* **2014**, *608*, 295−302, DOI: 10.1016/j.cplett.2014.05.069.
(77) Liu, S.; Comer, J.; van Duin, A. C. T.; van Duin, D. M.; Liu, B.; Edgar, J. H. Predicting the Preferred Morphology of Hexagonal Boron Nitride Domain Structure on Nickel from ReaxFF-based Molecular Dynamics Simulations. *Nanoscale* **2019**, *11*, 5607−5616, DOI: 10.1039/C8NR10291K.
(78) Karpinski, J.; Kazakov, S.; Jun, J.; Angst, M.; Puzniak, R.; Wisniewski, A.; Bordet, P. Single Crystal Growth of MgB_2 and Thermodynamics of Mg-B-N System at High Pressure. *Phys. C: Supercond.* **2003**, *385*, 42−48.
(79) He, D.; Akaishi, M.; Scott, B. L.; Zhao, Y. Growth of Boron Suboxide Crystals in the B-B2O3 System at High Pressure and High Temperature. *J. Mater. Res.* **2002**, *17*, 284−290.
(80) Vitry, V. Electroless Nickel-boron Deposits: Synthesis, Formation and Characterization. Ph.D. thesis, Université de Mons, Mons: Belgium, 2009.
(81) Xu, J.; Wei, B. Liquid Phase Flow and Microstructure Formation during Rapid Solidification. *Acta Phys. Sin.* **2004**, *53*, 1909−1915, DOI: 10.7498/aps.53.1909.
(82) Zhai, Q.; Xu, J.; Lu, T.; Xu, Y. Research on Interlayer Alloys for Transient Liquid Phase Diffusion Bonding of Single Crystal Nickel Base Superalloy DD6. *J. Mater. Sci. Chem. Eng.* **2014**, *02*, 12 DOI: 10.4236/msce.2014.29002.
(83) Liu, L.; Wei, Z.; Chen, Q.; Shen, C.; Shen, T.; Tian, X.; Li, S.-D. Benchmarking Boron Cluster Calculations: Establishing Reliable Geometrical and Energetic References for B_n (n = 1−4). *J. Comput. Chem.* **2024**, *45*, 159−169.
(84) Joshi, R. P.; McNaughton, A.; Thomas, D. G.; Henry, C. S.; Canon, S. R.; McCue, L. A.; Kumar, N. Quantum Mechanical Methods Predict Accurate Thermodynamics of Biochemical Reactions. *ACS Omega* **2021**, *6*, 9948−9959.
(85) Tran, A. L.; Guidez, E. B. Quantum Mechanical Modeling of the Interactions between Noble Metal (Ag and Au) Nanoclusters and Water with the Effective Fragment Potential Method. *ACS Omega* **2020**, *5*, 7446−7455.